Estimation of the Angle of Incidence based on Echo Pulse Width in Airborne LiDAR

JAN RHOMBERG-KAUERT[1], FLORIAN PÖPPL[1], MARTIN PFENNIGBAUER[2] & GOTTFRIED MANDLBURGER[1]

Abstract: As Airborne and UAV LiDAR have become widely used techniques to map large quantities of terrestrial and bathymetric landscapes, the extraction of more data from the returned signal is an important topic of research. Improvement in LiDAR sensors enable detailed detection of the returned laser pulse, which opens up the opportunity to extract more information from the recorded full signal waveform than ever before. Compared to infrared lasers, green LiDAR typically exhibits a significantly shorter wavelength, which in turn requires a wider footprint on the ground, as eye safety becomes a non-neglectable concern. Together with the typically shorter pulse duration, the bigger footprint is more susceptible towards a nonzero angle of incidence, as the change in reflecting area increases drastically with high angle of incidence. This can be seen in the change of the return signal waveform, which decreases in amplitude and widens in length, as the angle of incidence increases. Based on these effects we can estimate a point-based angle of incidence using the width of the waveform, as there exists a proportionality between the width of the signal and the angle. This opens the possibility to derive surface normal information purely from analysing the reflected echo waveform without considering neighbourhood information. Therefore an improvement is made as more pointwise information can be extracted and furthermore computational resources can be conserved.

1 Introduction

The improvements in LiDAR signal processing create new applications in the field of full waveform analysis, as the resolution of the recorded echo pulse increases with the adoption of advancements in technology and methods development (ULLRICH et al. 2007).
This opens up new opportunities to extract more information from the returned pulses for each beam sent by the scanner. Thus the enhancement of information extracted from LiDAR measurements has attracted much attention, diving deeper into the analysis of full waveform signals and the quantities these signals contain about the scattering object. Current research in this area mostly focuses on infrared lasers, as these have smaller footprints and therefore are often more suited for measuring campaigns (ABED et al. 2012; PFENNIGBAUER et al. 2013; YANG et al. 2022). There, the correlation of angle of incidence and signal amplitude is well known and can be corrected for, because the return signal intensity decreases with one over the cosine of the angle of incidence (HARTZELL et al. 2015). Similar correlations are often researched concerning the echo pulse width. There the correlation between the angle of incidence and echo pulse width is of interest, as this creates the opportunity to use the full waveform analysis to estimate angles of incidence (ABED et al. 2012; PFENNIGBAUER et al. 2013).
Previous research in this field has shown that this correlation of echo pulse width and angles of incidence is hard to quantify in clear terms for infrared LiDAR (PFENNIGBAUER et al. 2013).

[1] TU Wien, Department für Geodäsie und Geoinformation, Forschungsbereich Photogrammetrie, A-1040 Wien, E-Mail: [jan.rhomberg-kauert, florian.poeppl, gottfried.mandlburger]@geo.tuwien.ac.at
[2] *RIEGL* Research Forschungsgesellschaft mbH, A-3580 Horn, Austria, E-Mail: mpfennigbauer@riegl.com

 DOI: 10.24407/KXP:1885287615

The most prominent challenge of this correlation is that a significant change in echo pulse width is mostly observed at high angles of incidence for infrared lasers. Therefore, improvements towards a distinct correlation, which would allow for a general estimation based on the recorded waveform, would enhance the current standard of attribute extraction of full waveform point clouds (BOLKAS 2019; KUKKO et al. 2008; PFENNIGBAUER et al. 2013; YANG et al. 2022).
The remainder of this article is structured as follows: In Section 2, we introduce the employed processing methods and provide details of the used study area and datasets. We present the results in Section 3 and discuss them critically in Section 4. The article ends with a summary and conclusion remarks in Section 5.

2 Methods and materials

2.1 Dataset

The datasets displaying the phenomenon, mentioned in the introduction, come from a green airborne LiDAR system with a wavelength of 532 nm. The dataset was acquired by a *RIEGL* VQ-880-GII topo-bathymetric laser scanner (Fig 1 A and B) while surveying an area in the region of Loosdorf in Lower Austria (MANDLBURGER et al. 2015). The region contains both manmade structures such as houses, which offer a wider variety of different angles of incidence and planar fields and roads, which can be used as a reference, as there is an abundance of points with similar angles of incidence. The used scanner supports full waveform recording (MANDLBURGER 2020), allowing for an extraction of the returned echo pulses for each point based on the samples recorded. Therefore, almost every point can be associated with a full waveform, allowing a detailed analysis for both the recorded waveforms and point cloud attributes.
The houses in Fig. 1 A and a close up of the same houses in panel B show the well-known phenomenon of changes in amplitude, depending on the angle of incidence, as the dataset was a acquired with a close to constant range (HARTZELL et al. 2015; KAASALAINEN et al. 2011). The laser points show high amplitudes where the roofs are angled towards the scanner and a lower amplitude on the other side. This is increased by the angling of the VQ-880-GII surveying of the area. The scanner has a circular, off-nadir, scanning angle, thus roofs angled towards the scanner display ideal condition for unchanged echo pulses. In addition to the amplitude, the returned echo pulse changes in width as well, depending on the angle of incidence in the green LiDAR measurements, as the footprint is drastically different, compared to infrared, to keep the laser measurements within eye safety regulations. Therefore, the waveform is more prone to change due to variation of the angle of incidence. The described changes can be seen on Fig. 1 C, displaying the differences of the reflected waveforms and indicating the correlation between angles of incidence and echo pulse width.

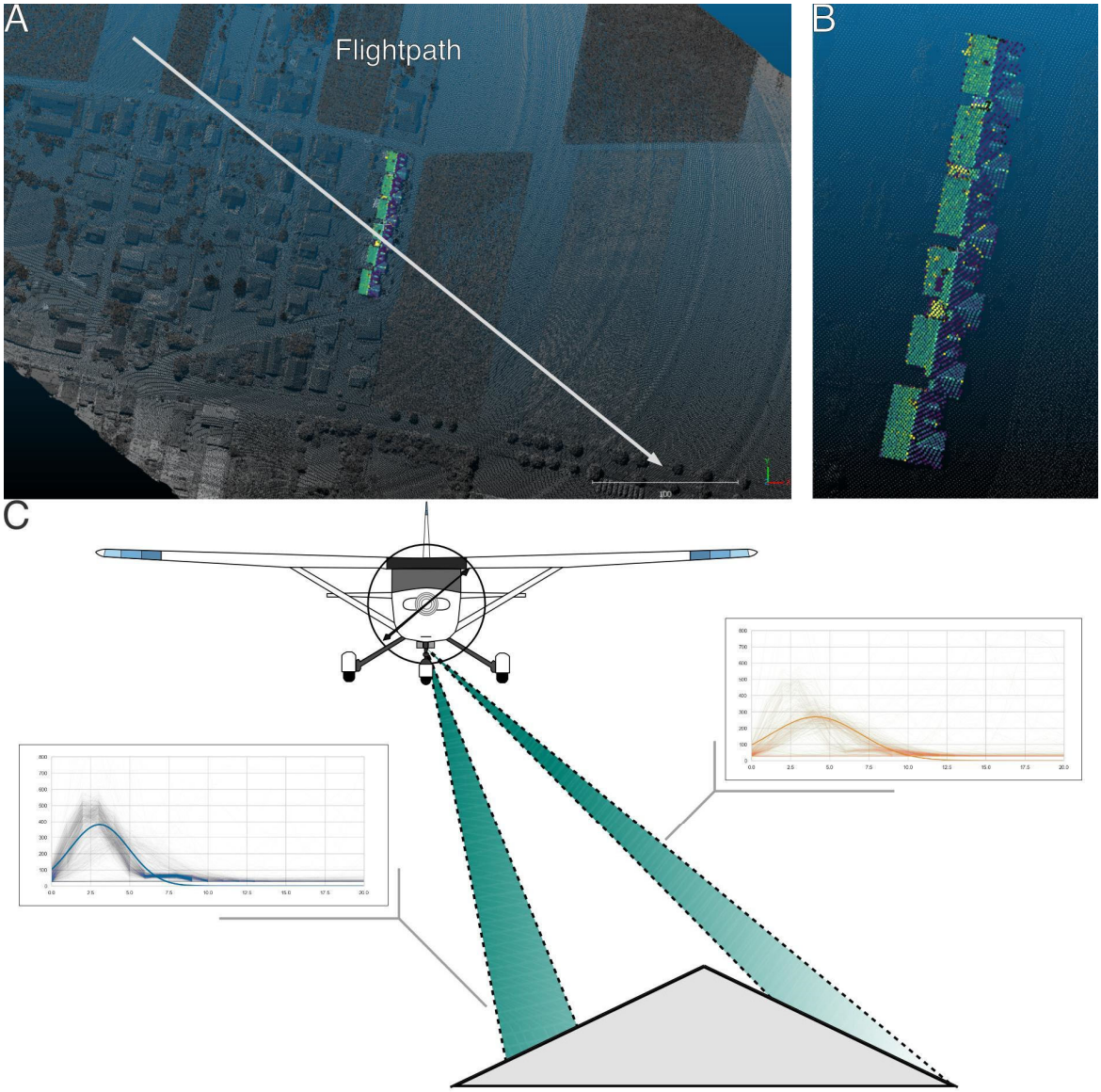

Fig. 1: (A) Plan view of a flight strip survey with the *RIEGL* VQ-880-GII (Loosdorf/Lower Austria). The white arrow shows the flight path of the aircraft and the houses are the selected data points coloured by amplitude. The *RIEGL* VQ-880-GII scanner is angled at 20° and has a circular scan pattern, which is visible in the figure looking at the even surface of the measured fields. (B) Zoomed in area of the Fig. shown in panel A, the houses used for illustration throughout the paper, referenced as the house dataset. (C) Illustration of the measured angle incidence in green LiDAR and the difference in amplitude and echo width for different angles of incidence.

2.2 Full waveform simulation

To create a correlation curve for all angles without overfitting or overly smoothing, we turn to simulating the returned echo pulses. The basis for this simulation is the frequently cited study by CARLSSON et al. (2001). This article describes a detailed method for convoluting heavy tailed curves with an angle dependent function. We start by introducing the heavy tailed curve we use to simulate the signal pulse sent out by the laser scanner. This function is used instead of a Gaussian pulse as the waveform in reality is often less steep on the falling edge of the pulse, which is even more the case for green LiDAR devices (HARTZELL et al. 2015). Therefore we get the heavy tailed curve p(t) as

$p(t) = \left(\frac{t}{\tau}\right) \cdot e^{\frac{-t}{\tau}}$, where $\tau = \frac{T_{\frac{1}{2}}}{3.5}$ and $T_{\frac{1}{2}}$ is the Full Width Half Maximum (FWHM).

Furthermore, we can describe the angle dependent return signal as the convolution of a Gaussian pulse with an angle dependent function, by improving upon the original equation from CARLSSON et al. (2001). This equation is described in the paper as

$$h(t) = e^{-\left(\frac{t-t'}{\tau_0}\right)^2}, \text{ where } t' = \frac{2 \cdot x_0}{c \cdot cos(\alpha)} \text{ and } \tau_0 = \frac{w \cdot \sqrt{2}}{sin(\alpha)}.$$

There x_0 is the footprint radius at the target, w is the beam divergence, $\boldsymbol{\alpha}$ is the angle of incidence and c is the speed of light (Fig. 2 A). The original angle dependent function of CARLSSON et al. (2001) was not suited for our estimation as the difference compared to real world data did not indicate a suited fitting (Fig. 3). Therefore, we applied a different transformation for the angle dependent function and henceforth obtained a different function for the angle dependency of the reflected echo pulse (Fig. 2 B). The applied transformation resulted in the flowing angle dependent function

$$\tilde{h}(t) = cos(\alpha) \cdot \sqrt{\pi} x_0 \cdot \frac{c}{sin(\alpha)} e^{-\left(\frac{ct}{x_0 tan(\alpha)}\right)^2},$$

where x_0 is the footprint radius, $\boldsymbol{\alpha}$ the angle of incidence and c the speed of light. By calculating the convolution of a heavy tailed curve with the angle dependent function, we can now simulate the echo pulse for each angle. The reflected echo pulse is therefore defined as

$$p_{reflected}(t) = \left(p * \tilde{h}\right)(t) = \int_0^t p(\xi) \cdot \tilde{h}(t - \xi) d\xi.$$

The calculated function enables a detailed simulation of all full waveforms for each angle of incident and can thus be used for further analysis, setting the stage for the angle estimation. The simulation of these echo pulses for each angle can be seen in Fig. 2 here we can clearly see an increase in echo pulse width with increasing angle of incidence.

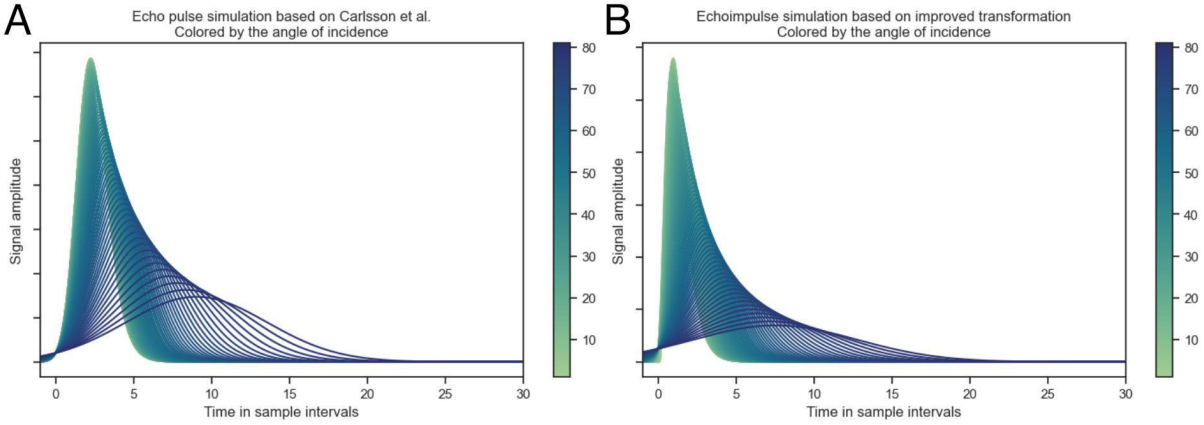

Fig. 2: (A) Simulated echo pulses based on the CARLSSON et al. (2001) article. Each curve represents the convolution of the heavy tailed curve with the angle dependent function, coloured by the corresponding angle of incidence. (B) Simulated echo pulses based the convolution of the differently transformed angle dependent function, coloured by the angle of incidence.

2.3 Angle estimation

Using the simulated echo pulses, we can analyse the different waveforms displayed in Fig. 2 and plot the signal width over the angle of incidence (Fig. 3), showing an exponential increase in echo pulse width with increasing angle of incidence. Building upon these results, we can now create a method for the angle of incidence estimation, which takes the echo pulse width

alone as a basis for angle determination without any neighbourhood information. For the estimation, we measure the echo pulse width at e^{-2} and match this with the simulated curve, creating a lookup table, where each width corresponds to a unique angle. This creates a single source angle of incidence estimation, without the need for neighbourhood calculations and plane fitting. This expands the advantages of full waveform analysis and overcomes challenges in neighbourhood parameter selection.

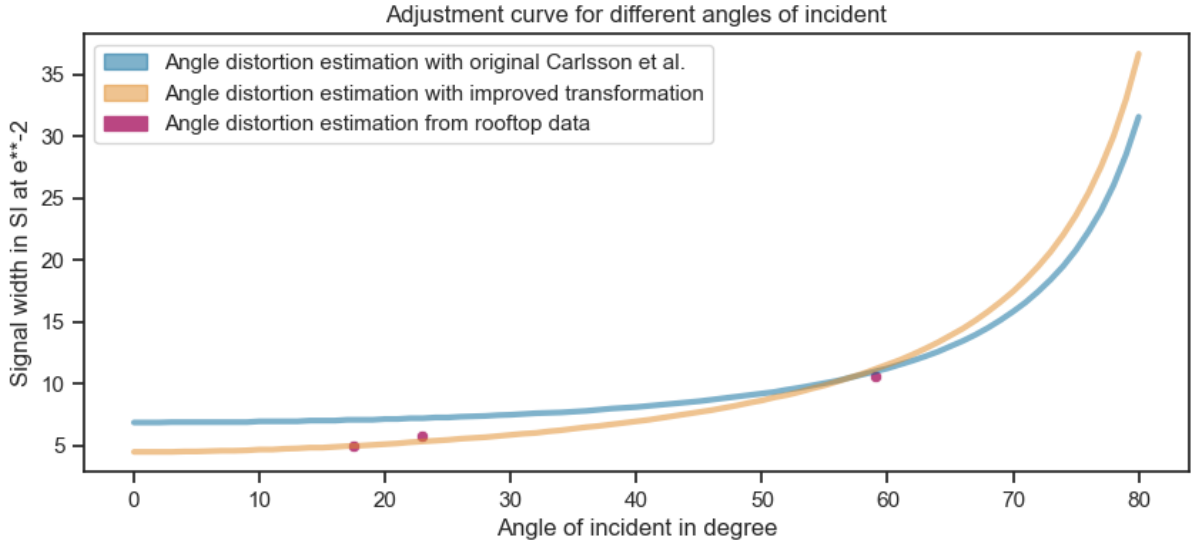

Fig. 3: The line plots display the correlation curve of the simulated echo pulse width, at maximum amplitude divided by e^{-2}, and the angle for each simulated echo. The blue curve is based on the original function by CARLSSON et al. (2001) and the orange one used the improved transformation for the angle dependent function. The pink dots represent ground truth extracted from the house dataset to put the simulation into a frame of reference

As the recorded echo is generally not oversampled enough to calculate the echo pulse width directly from the recorded samples we first have to fit a Gaussian pulse into the recorded signal samples. This has become a standard practice in the signal processing of recorded waveforms. Besides a Gaussian pulse, there exists a variety of different curves suited for such a fitting, especially heavy tailed curves as used in the simulation (CARLSSON et al. 2001; CHAUVE et al. 2007). The problem with such curves is that for long echo pulses the sampling frequency is too low to allow for well fitted heavy tailed curves, therefore Gaussian fitting was selected, as these curves displayed the most robust overall fitting, for all angles.
Using the continuous curves of the fitted Gaussian pulse, we can now extract an echo pulse width for each full waveform record in the dataset. Based on these extracted echo pulse widths at e^{-2}, an angle of incidence can be estimated for each waveform using the correlation curve shown in Fig. 3. This constitutes a new angle of incidence estimation method utilizing full waveform analysis only.

3 Results

The previously created simulation builds a broad basis for application related to the angle of incidence estimation, as we can now apply this correlation curve towards real world data and use it to estimate angles of incidence for airborne LiDAR. These estimations can then be compared to current best practices, i.e. dedication of incidence angle based on estimation of surface

normal from neighbouring laser points, e.g. using the scientific laser scanning software OPALS (PFEIFER et al. 2014). In our use case example, we used the module opalsNormals with standard parameters and estimated the surface normal angles from the nearest neighbours within a maximum search radius of 1 m. These normal vectors can then be combined with the laser beam vectors, derived from the flight trajectory and the measured can angles to calculate the angle of incidence. Plotting this for the house dataset, we can see that this works well for even surfaces. Limited accuracy is observable at the borders between two differently angled segments (Fig. 4). This could potentially be overcome by better parameter selection for the surface normal calculation, as robust fitting is already being used, which would require a supervised workflow and therefore more time during the analysis.

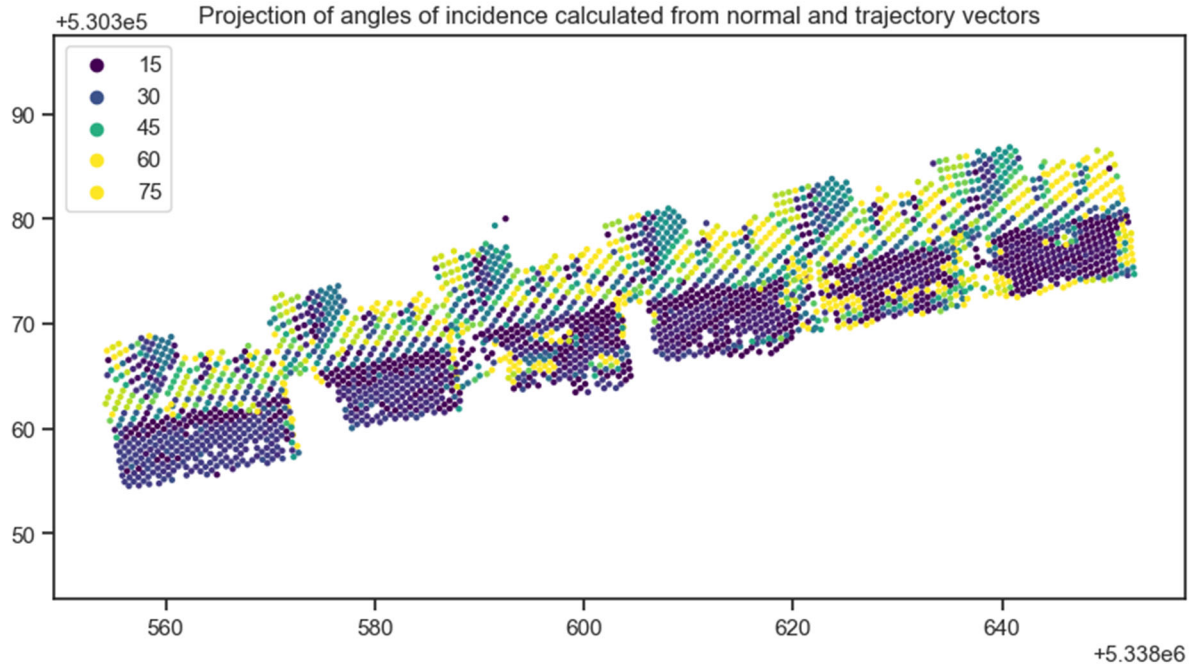

Fig. 4: Plane view of the house dataset coloured by the calculated angle of incidence. Each angle is calculated from the angle between the point's normal vector and the laser's trajectory vector for that point. In this case the angels were calculated using opalsNormals (PFEIFER et al. 2014)

On the other hand using the full waveform analysis, we can create an unsupervised method without parameters. By applying the created estimation method to the same dataset (Fig. 5), we can see that this is not prone to changes in the surface, therefore improving on surfaces where the local point neighbourhood is curved. This is a result of the single point attribute creation, which does not rely on neighbourhood information and only requires minimal curvature within the footprint,

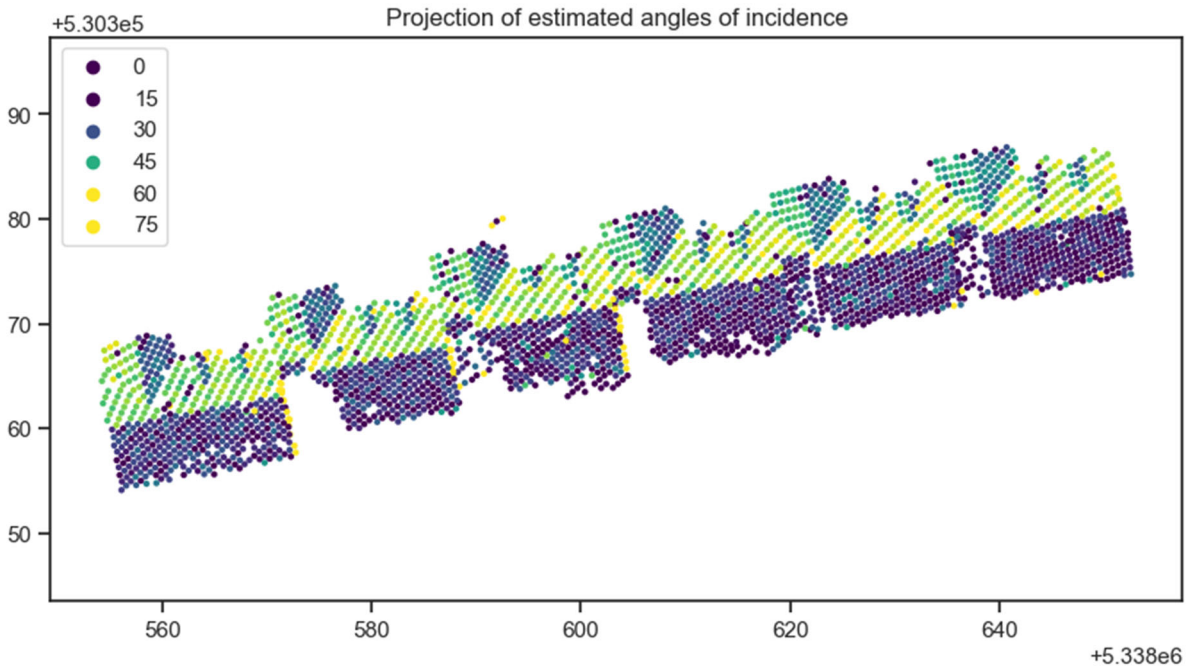

Fig. 5: Plane view of the house dataset coloured by the estimated angles of incidence based on the echo pulse width of the echo at e^{-2}

4 Discussion

The calculated and estimated angles of incidence (Fig. 4 and 5) can now be compared to get a deeper understanding of the advantages and disadvantages of both methods. This comparison is plotted in Fig. 6, displaying a high similarity between both methods, with the exceptions of the estimated angles close to zero. These are outliers from the estimation method as the waveforms are not always ideally recorded nor perfectly reflected. This results in recorded sample points not suited for Gaussian fitting. Leading to a deviation from the true echo pulse width, which in turn leads to a mismatched angle of incidence estimation.

On the other hand, the surface normal estimation using OPALS (PFEIFER et al. 2014) may need some parameter fine-tuning to achieve better results, therefore requiring more time to be spent on the post processing of the dataset. A direct comparison of both methods is therefore difficult to evaluate, as the recorded waveform is subject to different measuring conditions. These in turn influence the recorded waveform and thus a high sampling rate might be needed to improve the Gaussian fitting in suboptimal conditions (DONEUS & BRIESE 2006). Therefore, this new estimation method can be used to enhance existing workflows and thus improve neighbour-based algorithms in areas of high curvature and provides a new laser scanning attribute solely derived from the sensor data.

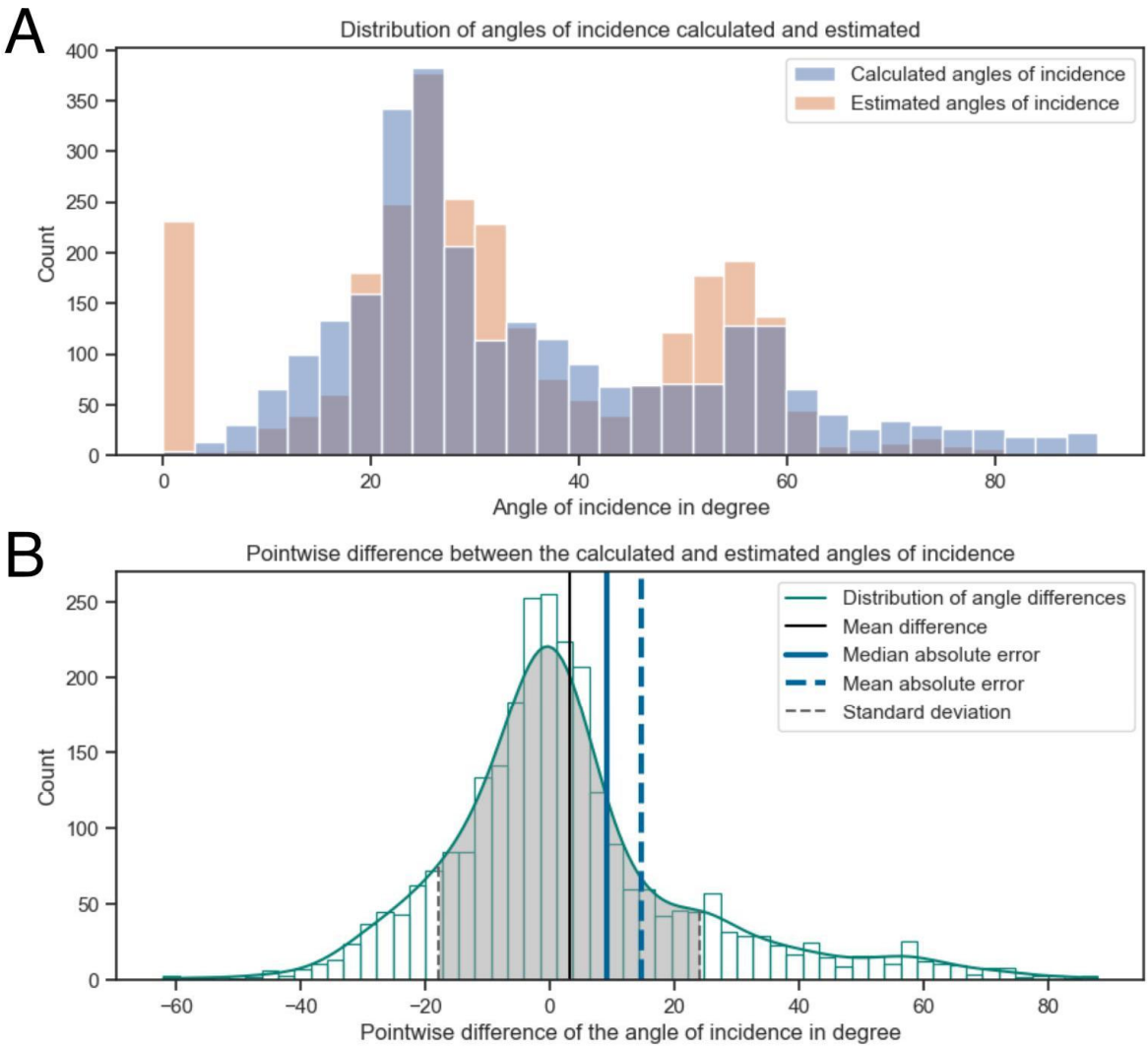

Fig 6: (A) Histogram of the calculated angles of incident, using normal vectors and the beam trajectory by OPALS (PFEIFER et al. 2014) and the estimated angles of incidence based on the echo pulse width and the correlation curve from the improved CARLSSON et al.(2001) simulation. (B) Histogram with distribution plot of the pointwise differences between the calculated and estimated angle of incidence. Furthermore, the plot shows the mean differences of the angles, the black line, and the mean and median absolute error, the two blue lines.

5 Conclusion

Using the full waveform analysis to extract additional points can therefore expand and improve other laser scanning applications besides airborne LiDAR. The application of full waveform analysis can especially be useful when commonly used techniques such as plane fitting for normal vector extraction are limited due to curvature of the surface or low point density (LI et al. 2012; ROCA-PARDIÑAS et al. 2014; STAŁOWSKA et al. 2022). Therefore using full waveform analysis to estimate incidence angles could improve the accuracy of such measurements.
Furthermore, the newly introduced methods would solely need the sensor data for further LiDAR attribute creation. Implementing an independent measure, which would not rely on neighbourhood selection. Allowing not only for angle estimation, but also for future research on reflectance values and potential ranging corrections, where the echo pulses get deformed due

to high angles of incidence. Concluding the introduced method creates new spaces for advancements of existing methods and can help improve accuracy where plane fitting would result in suboptimal angle of incidence calculations.

6 References

CARLSSON, T., STEINVALL, O. & LETALICK, D., 2001: Signature simulation and signal analysis for 3-D laser radar. FOI-R--0163--SE, E7030. Linköping: FOI - Swedish Defence Research Agency, https://www.foi.se/rest-api/report/FOI-R--0163--SE, letzter Zugriff 02.02.24.

ABED, F. M., MILLS, J. P. & MILLER, P. E., 2012: Echo Amplitude Normalization of Full-Waveform Airborne Laser Scanning Data Based on Robust Incidence Angle Estimation. IEEE Transactions on Geoscience and Remote Sensing, IEEE Geoscience and Remote Sensing Society, **50**(7), 2910-2918.

BOLKAS, D. 2019: Terrestrial laser scanner intensity correction for the incidence angle effect on surfaces with different colours and sheens. International Journal of Remote Sensing, https://doi.org/10.1080/01431161.2019.1601283.

CHAUVE, A., MALLET, C., BRETAR, F., DURRIEU, S., PIERROT-DESEILLIGNY, M. & PUECH, W. 2007: Processing full-waveform lidar data: Modelling raw signals. ISPRS Workshop Laser Scanning and SilviLaser (LS SL), **36**(Part 3/W52), 102-107.

DONEUS, M. & BRIESE, C., 2006: Full-waveform airborne laser scanning as a tool for archaeological reconnaissance. https://publik.tuwien.ac.at/files/PubDat_120639.pdf, letzter Zugriff 02.02.24.

HARTZELL, P. J., GLENNIE, C. L. & FINNEGAN, D. C., 2015: Empirical waveform decomposition and radiometric calibration of a terrestrial full-waveform laser scanner. IEEE Transactions on Geoscience and Remote Sensing: A Publication of the IEEE Geoscience and Remote Sensing Society, **53**(1), 162-172.

KAASALAINEN, S., JAAKKOLA, A., KAASALAINEN, M., KROOKS, A. & KUKKO, A., 2011: Analysis of Incidence Angle and Distance Effects on Terrestrial Laser Scanner Intensity: Search for Correction Methods. Remote Sensing, **3**(10), 2207-2221.

KUKKO, A., KAASALAINEN, S. & LITKEY, P., 2008: Effect of incidence angle on laser scanner intensity and surface data. Applied Optics, **47**(7), 986-992.

LI, X., XU, L., TIAN, X. & KONG, D. 2012: Terrain slope estimation within footprint from ICESat/GLAS waveform: model and method. Journal of Applied Remote Sensing, **6**(1), 063534.

MANDLBURGER, G., 2020: A review of airborne laser bathymetry for mapping of inland and coastal waters. Hydrographische Nachrichten, **116**(06/2020), 6-15.

MANDLBURGER, G., HAUER, C., WIESER, M. & PFEIFER, N. 2015: Topo-Bathymetric LiDAR for Monitoring River Morphodynamics and Instream Habitats - A Case Study at the Pielach River. Remote Sensing, **7**(5), 6160-6195.

PFEIFER, N., MANDLBURGER, G., OTEPKA, J. & KAREL, W. 2014: OPALS – A framework for Airborne Laser Scanning data analysis. Computers, Environment and Urban Systems, **45**, 125-136.

PFENNIGBAUER, M., WOLF, C. & ULLRICH, A. 2013: Enhancing online waveform processing by adding new point attributes. Laser Radar Technology and Applications XVIII, **8731**, 26-34.

ROCA-PARDIÑAS, J., ARGÜELLES-FRAGA, R., DE ASÍS LÓPEZ, F. & ORDÓÑEZ, C. 2014: Analysis of the influence of range and angle of incidence of terrestrial laser scanning measurements on tunnel inspection. Tunnelling and Underground Space Technology, **43**, 133-139.

STAŁOWSKA, P., SUCHOCKI, C. & RUTKOWSKA, M. 2022: Crack detection in building walls based on geometric and radiometric point cloud information. Automation in Construction, **134**, 104065.

ULLRICH, A., STUDNICKA, N., HOLLAUS, M., BRIESE, C., WAGNER, W., DONEUS, M. & MÜCKE, W. 2007: Improvements in DTM generation by using full-waveform airborne laser scanning data. Proceedings, **20**, 9.

YANG, T., LAI, J., WANG, C., YAN, W., JI, Y., ZHAO, Y., WU, Z. & LI, Z. 2022: Influence of a target's inclination on LiDAR waveform and its application. IET Optoelectronics, **16**(1), 27-33.